Hindawi
Advances in Civil Engineering
Volume 2018, Article ID 4071732, 21 pages
https://doi.org/10.1155/2018/4071732

*Research Article*

# Analysis Method for Reinforcing Circular Openings in Isotropic Homogeneous Plate-Like Structures Subjected to Blast Loading

**Sebastian Mendes and Liling Cao**

*Thornton Tomasetti, 40 Wall Street, 18th Fl., New York, NY 10005, USA*

Correspondence should be addressed to Sebastian Mendes; smendes@thorntontomasetti.com

Received 26 May 2018; Accepted 25 July 2018; Published 5 September 2018

Academic Editor: Chiara Bedon



An analysis method is formulated to predict the peak bending stress concentrations around a small circular opening in an idealized isotropic homogeneous, linear elastic-perfectly plastic plate-like structure subjected to uniform blast loading. The method allows for the determination of corresponding concentrated bending moments adjacent to the opening for the design of reinforcement that can prevent the formation of localized plasticity around the opening during a blast event. The rapid formation and growth of localized plasticity around the opening can lead to a drastic reduction of the plate-like structure's local and global stability, which could result in catastrophic failure of the structure and destruction of the entity it is protecting. A set of elemental formulas is derived considering one-way and two-way rectangular plate-like structures containing a single small circular opening located where flexure predominates. The derived formulas are applicable for elastic global response to blast loading. Abaqus was employed to conduct numerical verification of the derived formulas considering various design parameters including material properties, plate dimensions, position of opening, and explosive charge size. The formulas demonstrate a good correlation with FEA albeit with a conservative inclination. The derived formulas are intended to be used in tandem with dynamic SDOF analysis of a blast load-structure system for ease of design. Overall, the proposed method has the potential to be applicable for many typical conditions that may be encountered during design.

## 1. Introduction

Plate-like structures are often used in buildings to protect occupants and life-safety systems from high-energy explosions [1]. Examples of plate-like structures include hardened blast walls and strengthened floor slabs for protecting against blast infill pressure. Hardened blast walls are strategically positioned within a building to protect means of egress and equipment critical for the functioning of life-safety systems after the blast event. The blast walls are nonload bearing and designed to resist blast infill pressure by one-way flexural behavior. Strengthened floor slabs are located in building areas where prevention of floor collapse is determined to be imperative in thwarting progressive collapse after the blast event [1]. The floor slabs are designed to carry conventional gravity and diaphragm loads while also resisting blast infill pressure by two-way or one-way flexural behavior.

A rational approach to the blast-resistant design of structures was articulated by Newmark in 1956 [2] and Biggs in 1964 [3]. Since that time, the performance of various civil structures such as reinforced concrete frames, reinforced masonry walls, and timber panels subjected to blast loading has been investigated [4–6]. Importantly, the performance of the building envelope, essentially glazing and glass facades, under air blast has been researched [7, 8]. In direct relation to this paper, the dynamic behavior of metallic plate-like structures subjected to blast loading has been extensively investigated through analytical, numerical, and experimental studies [9–18]. At present, blast-resistant design is standardized in several publications including ASCE 59-11 *Blast Protection of Buildings* [1] and UFC 3-340-02 *Structures to Resist the Effects of Accidental Explosions* [19]. The global dynamic response of plate-like structures can remain in the elastic regime, or in extreme cases can enter the plastic

regime. The dynamic response is in part dependent upon the structural material, support conditions, explosive charge weight, standoff, and the ratio of the reflection surface to the target area [1, 3, 19].

Plate-like structures designed for blast loading are often required to have circular penetrations to accommodate mechanical ducts or electrical conduits. The size and positioning of the penetrations depends upon the function of the entity being protected. For example, a steel hardened blast wall protecting a communication room within a building may require a small circular opening to accommodate electrical conduits. The presence of a small circular opening in a plate-like structure undergoing out-of-plane deformation due to blast loading induces especially high bending stress concentrations around the opening, as demonstrated in Figures 1(a) and 1(b). These stress concentrations can cause localized plasticity even though the initial global response of the structure primarily remains in the elastic strain range. The rapid formation and growth of localized plasticity around the opening can lead to a drastic reduction of the plate-like structure's local and global stability, which could result in catastrophic failure of the structure and destruction of the entity it is protecting. Reinforcement can be added to strengthen the region around the opening to resist bending stress concentrations that can cause localized plasticity, as shown in Figure 1(c).

There is a considerable amount of literature pertaining to stress concentrations around flaws subjected to far-field stress. The plane solution for stress concentrations around circular openings was derived by Kirsch in 1898 [20]. Stress concentrations at cracks were later investigated by Griffith, Westergaard, and Irwin [21–23]. More recent studies have investigated stress concentrations around irregularly shaped holes and circular holes in anisotropic materials [24–30]. The influence of openings on stability has been investigated [31–33].

A high-energy explosion is characterized by a rapidly expanding hemispherical wave of high-pressure gas called a shock wave. The reflected pressure and impulse from the shock wave upon or within a structure is a primary cause of damage from blast effects [19]. The reflected pressure and impulse are dependent upon several parameters including the explosive charge weight, range to target, angle of incidence, and shielding effects from the building façade or any intermediate partition walls [1]. The reflected pressure can be described by a pressure-time history curve, where the positive area beneath the curve is the reflected blast impulse. A blast pressure-time history curve is characterized by a sharp increase in positive pressure followed by a nearly linear decay to atmospheric pressure, as shown in Figure 2(a). A simplified triangular pressure-time history curve can be constructed from the peak reflected pressure and impulse for use in design, as shown in Figure 2(b) [1].

The blast impulse imparts inertial energy into a structure, causing it to undergo dynamic deformation [3]. In the case of plate-like structures, the blast impulse causes the structure to rapidly deform out-of-plane wherein the deformation response of the structure is dependent upon its flexural stiffness, ultimate resistance, mass, and inherent structural damping. The structure continues to oscillate in free vibration after the blast pressure has dissipated provided the structure remains intact. For all practical purposes, the deformation response corresponds to the fundamental mode with the mechanical energy balance oscillating between kinetic energy and internal strain energy [3, 19].

A common industry standard analysis method for designing structural elements for blast loading is to transform the load-structure system into an equivalent undamped single degree-of-freedom ("SDOF") system possessing a linear elastic-perfectly plastic response mode [1, 19]. The system is loaded by a triangular pressure-time history curve representing the actual blast pressure-time history, as shown in Figures 3(a) and 3(b). This procedure involves employing factors to transform the load, stiffness, ultimate resistance, and mass into equivalent values for use in an SDOF analysis such that the displacement response remains consistent between the real and equivalent systems [3]. The transformation factors are in part dependent upon the deformed shape and boundary conditions of the plate-like structure. The displacement response of the SDOF system can be solved for using various numerical methods such as the constant-velocity procedure. Peak stresses occur very early in the displacement response, and thus, inherent structural damping can be neglected in the analysis.

The structural properties of a plate-like structure can be designed to optimize its strength and performance for a given blast loading scenario. For reasons of practicality, a structure can be designed to resist the peak forces experienced during the free vibration phase while maintaining prescribed performance requirements. Performance requirements generally allow a structure to attain certain levels of ductility and deformation depending upon its structural composition. Maximum response limits for structural components subjected to blast effects are recommended by ASCE 59-11 [1].

In designing a plate-like structure containing a small circular opening for blast effects, it may be desirable to approximately calculate the distribution of peak bending stress around the opening such that suitable reinforcement can be designed to resist stress concentrations that can cause localized plasticity. The response of the plate-like structure may be adversely influenced if any localized plasticity around the opening is allowed to form and grow over subsequent cycles of free vibration. Specifically, the kinetic energy of the plate-like structure may be progressively dissipated or stored as plastic strain energy around the opening, potentially resulting in large deformations, rupture, or dynamic fracture during the initial cycle or subsequent oscillations, as depicted in Figure 4(b) [34–36]. The use of oversimplified analytical methods for calculating the stress concentrations may result in an overly conservative design of the reinforcement. Conversely, the use of complex analytical or computational methods can result in a more efficient design; however, these methods may be time-consuming and require a significant allotment of computational capacity thus rendering them impractical for design.

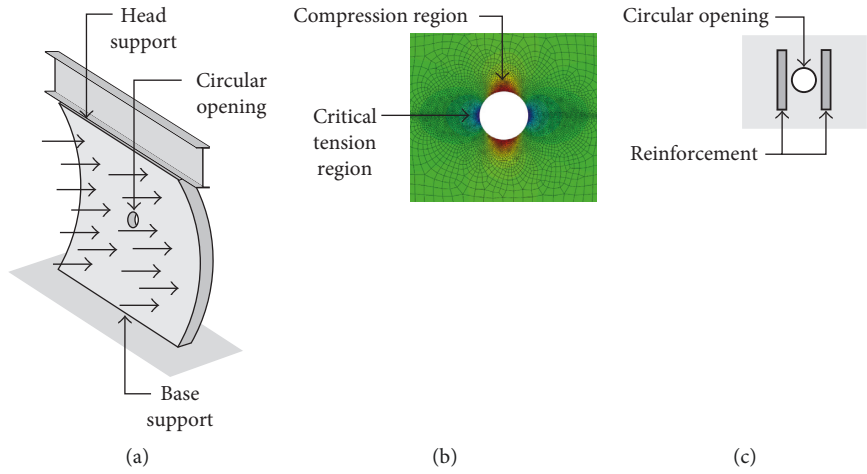


Figure 1: (a) One-way plate-like structure undergoing out-of-plane flexure due to blast loading; (b) bending stress concentrations around the opening; (c) reinforcement added around the opening.

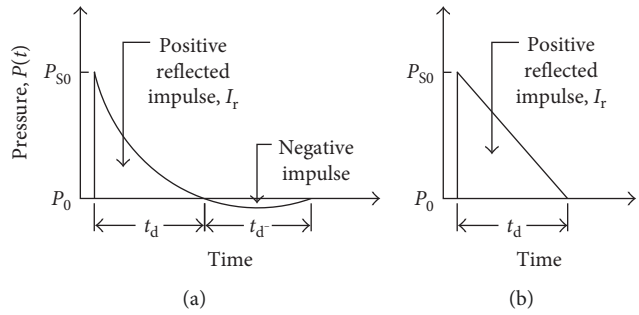


Figure 2: Blast pressure-time history curves: (a) typical blast pressure-time history curve; (b) simplified triangular blast pressure-time history.

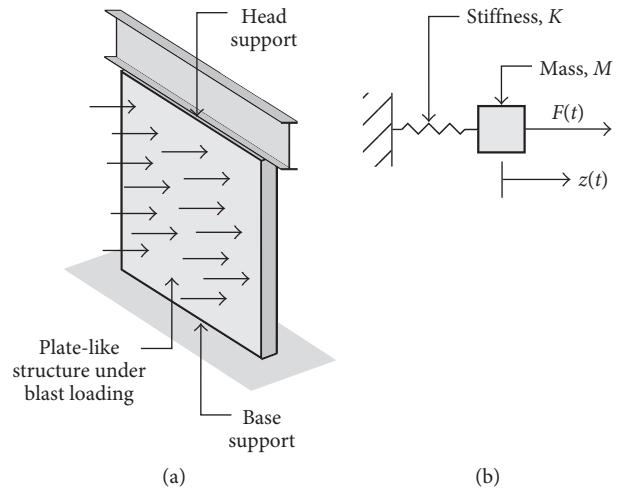


Figure 3: Load-structure system transformed into an equivalent undamped SDOF system for analysis of blast load response: (a) blast load-structure system; (b) equivalent undamped SDOF system.

## 2. Analysis Method

The objective is to formulate an analysis method to predict the peak bending stress concentrations around a small circular opening in an idealized isotropic homogeneous plate-like structure subjected to uniform blast loading. The predicted stress concentrations are to be used to design reinforcement that can prevent the formation of localized

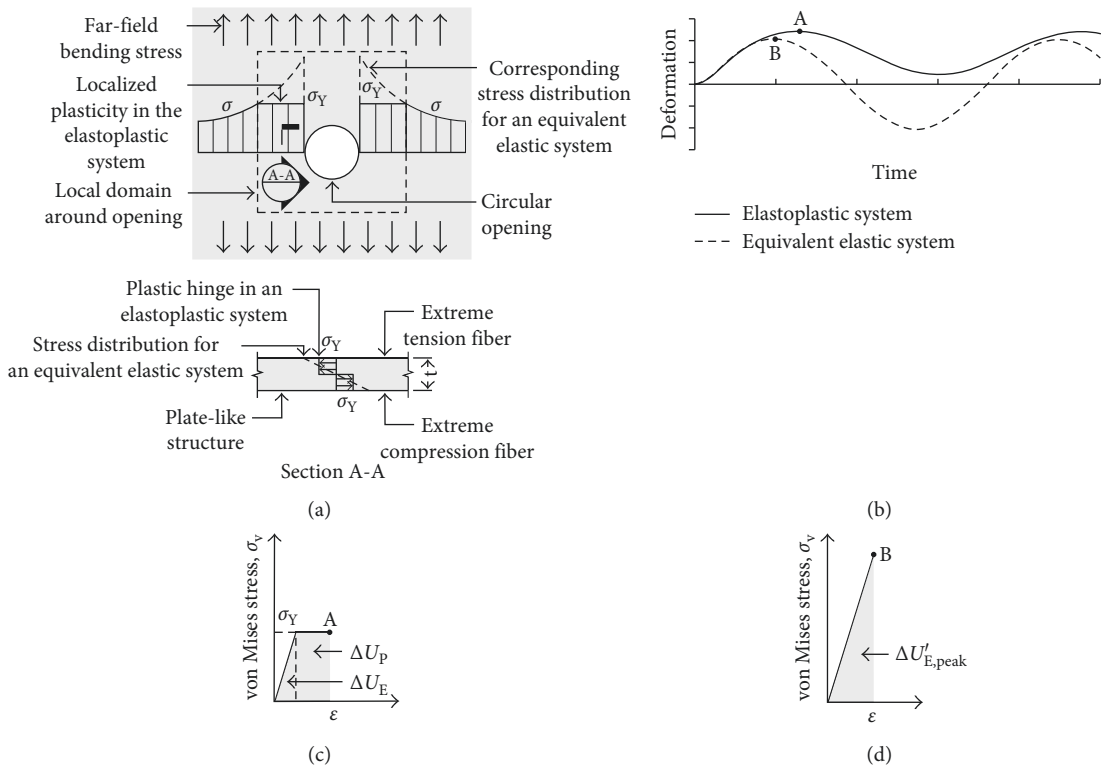


Figure 4: Peak stress concentrations and strain energy in the local domain around the opening for the elastoplastic system and equivalent elastic system during initial oscillation: (a) peak unidirectional stress concentrations adjacent to the opening and parallel to far-field bending stress; (b) deformation response for the elastoplastic system and equivalent elastic system; (c) peak elastoplastic strain energy developed in the local domain around the opening; (d) corresponding elastic strain energy developed in the same domain for the equivalent elastic system.

plasticity. The method is intended to be compatible with dynamic SDOF blast analyses of plate-like structures possessing elastic global response. In accordance with industry standards, the blast load-structure system is assumed to possess a linear elastic-perfectly plastic response mode for the localized stress concentrations around the opening [1].

The introduction of an opening in a plate-like structure inherently modifies its flexural stiffness. If the opening is small compared to the unbraced surface area of the structure free to deform out-of-plane, then the change in stiffness can be considered negligible (here, the definition of "small" is highly subjective upon the allowable change in dynamic response). Consequently, the global deformation response of a plate-like structure containing a small opening and subjected to blast loading is effectively unchanged from the response of an identical structure without an opening. This is true unless plastic hinges, rupture, or cracks develop adjacent to the opening such that the response is adversely influenced (Figure 4).

The failure criterion is defined as the formation of plasticity in the local domain around the circular opening, that is, the development of plastic hinges adjacent to the opening due to concentrated bending moments, as depicted in Figure 4(a). As per the principle of conservation of mechanical energy (neglecting structural damping), the total mechanical energy around the opening remains constant as the plate-like structure oscillates through out-of-plane deformation during free vibration [37]:

$$0 = \Delta U + \Delta K, \tag{1}$$

where $\Delta U$ is the internal strain energy in the local domain around the opening and $\Delta K$ is the associated kinetic energy imparted by the blast impulse. As the plate-like structure achieves its initial peak out-of-plane deformation, the kinetic energy is zero and the total mechanical energy around the opening is entirely strain energy:

$$\Delta U_{\text{peak}} = \Delta U_{\text{E}} + \Delta U_{\text{P}}, \tag{2}$$

where $\Delta U_{\text{E}}$ is the elastic strain energy and $\Delta U_{\text{P}}$ is the plastic strain energy. The formation of localized plasticity around the opening is indicated by the development of plastic strain energy and accompanying permanent deformation, as depicted in Figure 4(b). This permanent deformation can adversely influence the plate-like structure's local and global stability and subsequent response. Thus, the failure criterion is achieved when the plastic strain energy develops, expressed as follows:

$$\Delta U_{\text{P}} > 0. \tag{3}$$

Reinforcement around the opening should be designed to resist concentrated peak bending moments developing plastic hinges adjacent to the opening and corresponding to $\Delta U_{\text{peak}}$ when (3) is satisfied. In terms of strain energy, the reinforcement should be designed to absorb $\Delta U_{\text{peak}}$ in

a purely elastic form. In accordance with the principle of conservation of mechanical energy, the peak elastoplastic strain energy $\Delta U_{\text{peak}}$ around the opening during the first cycle of vibration is in the most conservative case effectively equal to the peak elastic strain energy, $\Delta U'_{\text{E,peak}}$, in the same domain derived from an equivalent *elastic* system, as depicted in Figures 4(c) and 4(d) [34, 35]. Thus, the concentrated peak bending moments can be solved by evaluating the bending moments corresponding to $\Delta U'_{\text{E,peak}}$:

$$\Delta U_{\text{E}} + \Delta U_{\text{P}} \approx \Delta U'_{\text{E,peak}}. \tag{4}$$

In general, the following formulation is proposed: in the first step a blast load-structure system is derived for a plate-like structure assumed to not contain a small circular opening. This is achieved by first constructing a triangular pressure-time history based on a given blast loading scenario. Next, the characteristic shape function and flexural stiffness are extracted from the assumed deformed shape of the plate-like structure corresponding to the fundamental mode. Mass and load transformation factors are then derived from the shape function, mass, and load. The blast load-structure system is transformed into an equivalent undamped SDOF system and dynamically analyzed in the elastic strain range. The peak displacement during the free vibration phase is extracted from the analysis.

In the intermediate step, the deformed shape is expressed in terms of the characteristic shape function and the peak displacement. The complete peak bending stress field at the tension surface of the plate-like structure may then be determined by substituting the deformed shape into the Kirchhoff–Love plate differential equations for expressing bending stresses in terms of curvatures.

In the final step, a small circular opening is assumed to lie within an infinite plane and loaded by uniaxial or biaxial far-field tensile stress. The tensile stress is determined from the bending stress field obtained in the previous step at the theoretical location of the opening. The Kirsch equations are used to determine the elastic stress concentrations around the circular opening when loaded by the far-field tensile stress (assuming no yielding). As a result, the peak elastic bending stress concentrations around a circular opening may in part be expressed in terms of the peak displacement obtained from a dynamic SDOF blast analysis in the elastic strain range. As per the principle of conservation of mechanical energy, the concentrated peak bending moments adjacent to the opening producing plastic hinges may be determined from the unidirectional elastic stress concentrations adjacent to the opening (and parallel to the far-field tensile stress) exceeding the actual yield point [37, 38]. This is under the propositions that the unidirectional elastic stress predominates the state of stress and is thus used in lieu of the von Mises stress, and that the elastoplastic transition range through the thickness is neglected. The resulting concentrated peak bending moments may then be used to design appropriate reinforcement for preventing localized plasticity around the opening.

Two common cases of rectangular plate-like structures are considered; a rectangular wall simply supported at two opposite edges, and a rectangular slab simply supported at all four edges. These two particular cases encompass a significant share of blast-resistant plate-like structures incorporated into buildings. Numerical verification of the analysis method is performed using the finite element analysis ("FEA") software Abaqus. The formulation of the analysis method is outlined in Figure 5.

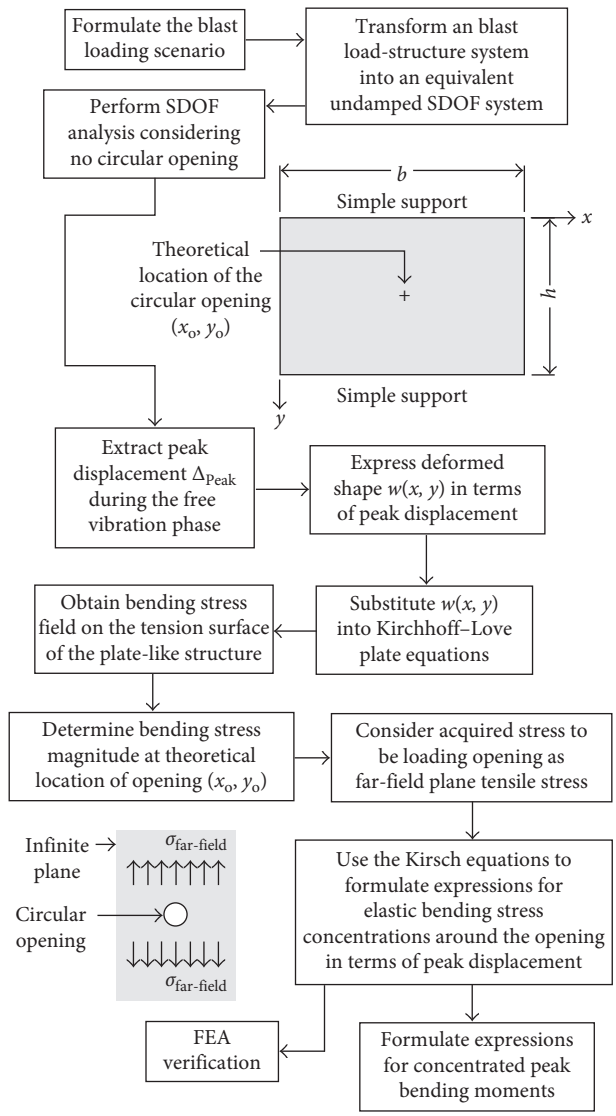


Figure 5: Proposed formulation of the analysis method.

*2.1. Case: Rectangular Wall Simply Supported at Two Opposite Edges.* It is assumed that the deformed shape of a rectangular plate-like structure during elastic response to blast loading conforms to the deflection surface obtained from a statically applied uniform surface load. Any deflection surface, $w(x, y)$, for an isotropic homogeneous plate-like structure must satisfy the boundary conditions and the governing plate equation [39]:

$$\nabla^4 w(x, y) = \frac{\partial^4 w}{\partial x^4} + 2\frac{\partial^4 w}{\partial x^2 \partial y^2} + \frac{\partial^4 w}{\partial y^4} = \frac{q}{D}, \tag{5}$$

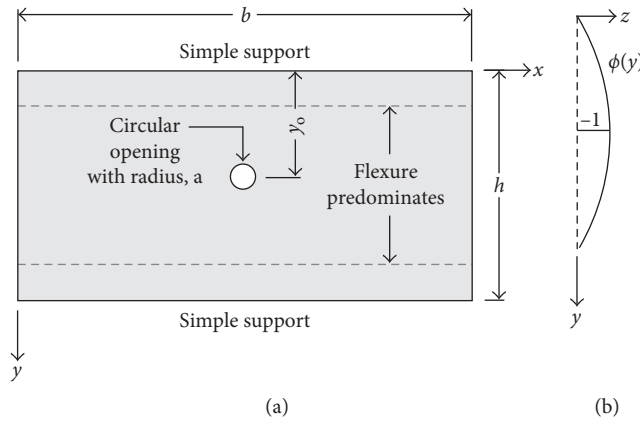


Figure 6: (a) One-way rectangular wall with a small circular opening under blast loading; (b) characteristic shape function.

Table 1: Parameters for an equivalent SDOF system of a one-way flexural element simply supported at the two opposite edges [3].

| Strain range | Real stiffness, $K$ | Mass factor, $K_M$ | Load factor, $K_L$ |
|---|---|---|---|
| Elastic | $(384EI)/(5h^3)$ | 0.50 | 0.64 |

where $q$ is the uniform surface load and $D$ is the plate flexural rigidity defined by $Et^3/[12(1-\mu^2)]$.

A rectangular wall simply supported at the two opposite edges and uniformly loaded by blast pressure effectively behaves as a one-way flexural element, where bending occurs in the $y$-axis direction between the supported edges. Parameters described with respect to the transverse $x$-axis direction remain constant and therefore vanish from the bending equations for the $y$-axis direction. A small circular opening is assumed located within the wall where flexure predominates. The one-way rectangular wall and its deformed shape under blast loading are shown in Figures 6(a) and 6(b).

The deformed shape, characteristic shape function, stiffness, and transformation factors for one-way flexural elements are readily available in the literature [3]. The deformation in the elastic strain range is described with respect to the $y$-axis in the direction of one-way bending and is given as follows:

$$w(y) = \frac{q}{24EI}\left(h^3 y - 2hy^3 + y^4\right), \tag{6}$$

where $h$ is the wall height, $E$ is Young's modulus, and $I$ is the second moment of area about the neutral axis. The corresponding characteristic shape function is expressed as follows:

$$\phi(y) = \frac{16}{5h^4}\left(h^3 y - 2hy^3 + y^4\right). \tag{7}$$

The well-known real stiffness and mass and load transformation factors for one-way flexural elements are listed in Table 1.

The parameters in Table 1 can be used to perform an equivalent SDOF analysis for a given blast loading scenario from which the peak displacement of the wall, $\Delta_{peak}$, can be extracted for deformations remaining within the elastic strain range.

In general, the peak deformed shape can be expressed in terms of the characteristic shape function and peak displacement as follows:

$$w_{peak}(x, y) = \Delta_{peak}\phi(x, y). \tag{8}$$

The Kirchhoff–Love plate differential equations for expressing bending stresses at the surface of a plate in terms of the peak deformed shape are given as follows [39]:

$$\sigma_x(x, y) = \frac{-tE}{2(1-\mu^2)}\left(\frac{\partial^2 w_{peak}}{\partial x^2} + \mu\frac{\partial^2 w_{peak}}{\partial y^2}\right), \tag{9a}$$

$$\sigma_y(x, y) = \frac{-tE}{2(1-\mu^2)}\left(\mu\frac{\partial^2 w_{peak}}{\partial x^2} + \frac{\partial^2 w_{peak}}{\partial y^2}\right), \tag{9b}$$

where $t$ is the wall thickness and $\mu$ is Poisson's ratio. Equations (9a) and (9b) can be used to approximate the far-field bending stress inducing stress concentrations around the small circular opening in the wall due to out-of-plane deformation. Substituting (7) into (8) and substituting the result into (9b) gives an expression for the bending stress $\sigma_y$ at the tension surface of the wall, in the direction of one-way flexure, and in terms of the peak displacement:

$$\sigma_y(y_o) = -\frac{96tE\Delta_{peak}\left(y_o^2 - hy_o\right)}{5h^4\left(1-\mu^2\right)}, \tag{10}$$

where $y_o$ is the location of the opening along the height of the wall. The transverse bending stress $\sigma_x$ is neglected for one-way flexure since its contribution to the stress concentrations around the opening is minute compared to the contribution by $\sigma_y$ [40].

Equation (10) can be used to approximate the uniaxial far-field bending stress at the tension surface of the wall and loading the circular opening, as shown in Figure 7. The plane elastic stress field around a circular opening loaded by uniaxial far-field tensile stress is expressed by the Kirsch equations in polar coordinates as follows [20]:

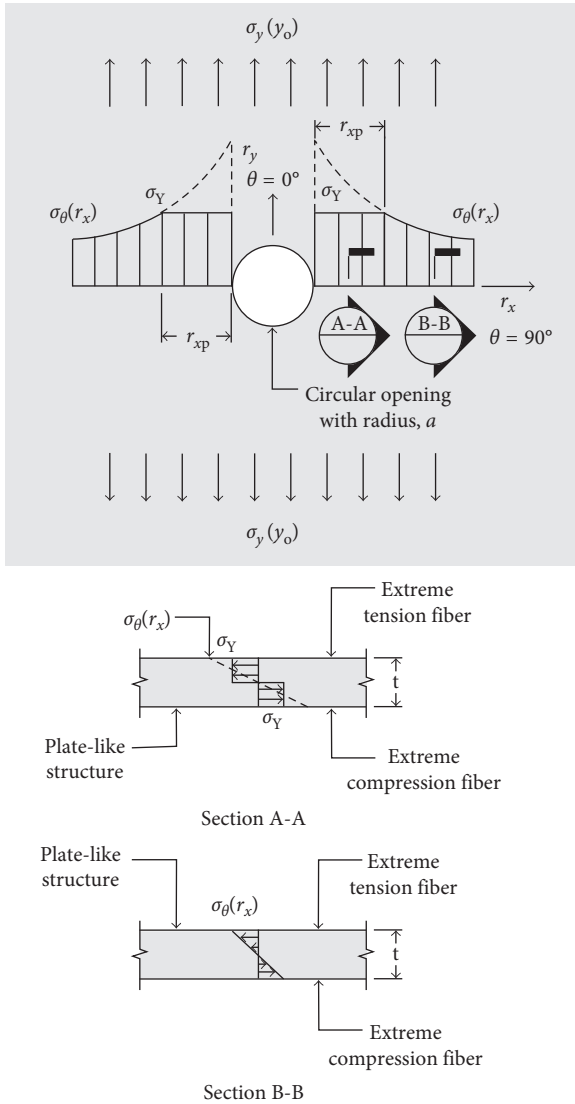


Figure 7: Far-field bending stress and resulting peak bending stress distribution along $r_x$ directly adjacent to the circular opening.

$$\sigma_\theta(r,\theta) = \frac{\sigma_\infty}{2}\left(1+\frac{a^2}{r^2}\right) - \frac{\sigma_\infty}{2}\left(1+\frac{3a^4}{r^4}\right)\cos(2\theta), \quad (11)$$

where $a$ is the radius of the opening, $r$ is the radial distance with respect to the center of the opening, $\theta$ is the angle with respect to the axis of far-field stress, and $\sigma_\infty$ is the uniaxial far-field tensile stress. In the case of one-way flexure, the peak elastic bending stress distribution, $\sigma_\theta(r_x)$, along the $r_x$ radial distance is principally induced by the far-field bending stress in the $y$-axis direction. Substituting (10) into (11) with $\sigma_\infty = \sigma_y$ and $\theta = 90^\circ$ results in an expression for the distribution of peak elastic bending stress at the tension surface of the wall and directly adjacent to the opening:

$$\sigma_\theta(r_x) = -\frac{48tE\Delta_{\text{peak}}\left(hy_o - y_o^2\right)\left(3a^4 + a^2r_x^2 + 2r_x^4\right)}{5\left(\mu^2-1\right)h^4r_x^4}, \quad (12)$$

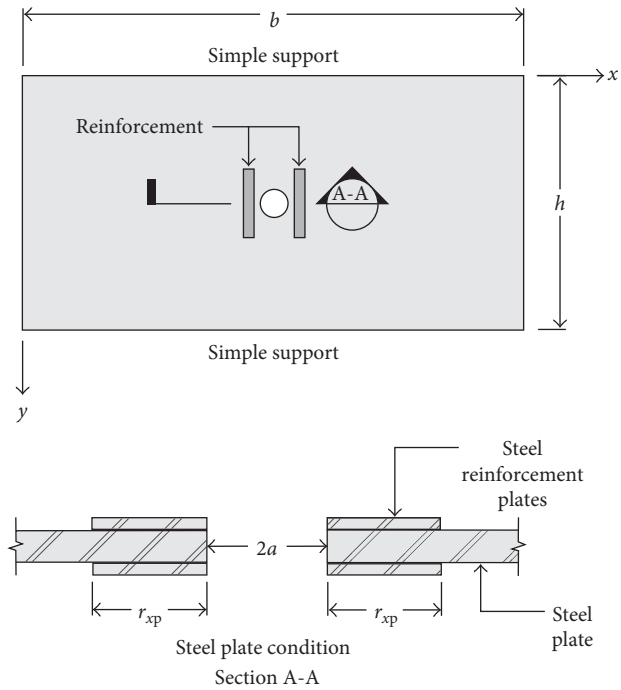


Figure 8: Reinforcement arrangement around the circular opening in the one-way rectangular wall.

where $r_x$ is the radial distance when $\theta = 90^\circ$. The peak elastic bending stress distribution along $r_x$ is depicted in Figure 7.

Localized plasticity around the opening occurs when the peak bending stress distribution at the tension surface exceeds the material yield strength, $\sigma_Y$. For reasons of simplicity, the elastoplastic transition range through the wall thickness is neglected and the presence of yielding at the wall surface is assumed to signify the development of a through-thickness plastic hinge, as shown in Figure 7. Reinforcement can be positioned around the opening in order to strengthen the regions of high bending stress concentrations where plastic hinges are expected to occur.

For the case of one-way flexure, reinforcement should be positioned on each side of the circular opening and oriented in the direction of one-way flexure such that the concentrated bending moments directly adjacent to the opening are effectively resisted, as shown in Figure 8. Each region of reinforcement should be designed to transfer the concentrated peak bending moment, $M_{xp}$, on each side of the opening such that yielding does not occur at the wall surface. In accordance with the principle of conservation of mechanical energy given by (4), the concentrated peak bending moment producing a plastic hinge can be determined by integrating the peak elastic bending stress distribution (assuming no yielding) over the radial distance over which yielding does occur and multiplying with the unit elastic section modulus:

$$M_{xp} = \frac{t^2}{6}\int_a^{r_{xp}+a} \sigma_\theta(r_x)\,dr_x, \quad (13)$$

where $r_{xp} + a$ is the radial distance at which $\sigma_\theta = \sigma_Y$. In summation form,

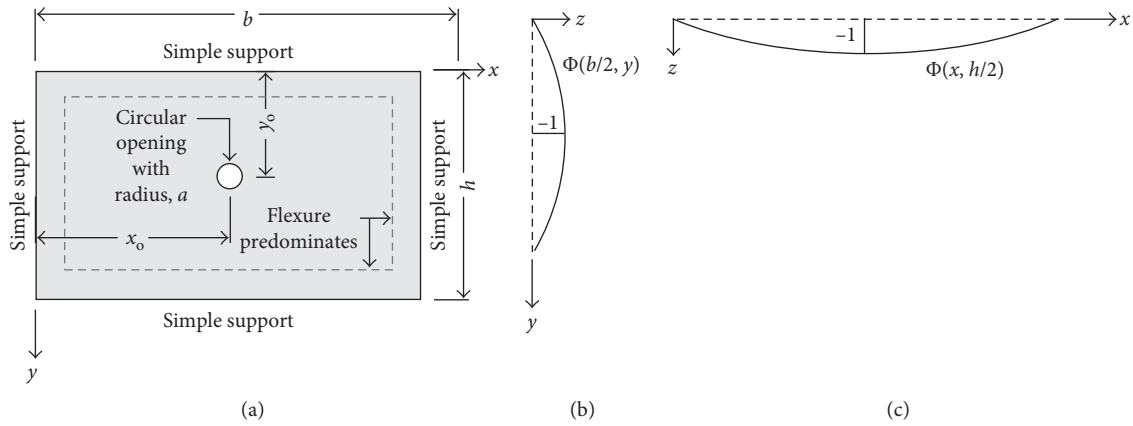


Figure 9: (a) Two-way rectangular slab with a small circular opening under blast loading; (b) shape function along the $y$-axis; (c) shape function along the $x$-axis.

$$M_{xp} = \frac{t^2}{6} \sum_{i=a}^{r_{xp}+a} \sigma_\theta (r_x)_i \Delta r_x. \tag{14}$$

The radial distance $r_{xp}$ over which yielding occurs can be solved by substituting the known constants into (12), setting the result equal to $\sigma_Y$, solving for $r_x$, and subtracting $a$. Equation (12) may then be substituted into (14) to obtain the concentrated peak bending moment. The summation term in (14) may be readily solved in spreadsheet form by summing the values of $\sigma_\theta$ at each incremental length $\Delta r_x$ along the radial distance $r_{xp}$.

The nominal *elastic* bending limit, $M_{nr}$, of a reinforced region directly adjacent to the opening should be equal to or greater than $M_{xp}$, explicitly expressed by the fundamental design requirement:

$$M_{nr} \geq M_{xp}. \tag{15}$$

The width of each reinforced region should nominally be equal to $r_{xp}$ and extend longitudinally at least beyond the extents of the opening, as shown in Figure 8. The elastic bending limit of the reinforced region is dependent upon the material and geometric properties of the reinforced section and may be readily determined from design formulas. In general, $M_{nr}$ is equal to an internal moment at which the extreme outer fibers of the reinforced section begin to yield, explicitly expressed by the product of the yield strength and the elastic section modulus, $S$, of the reinforced section [40]:

$$M_{nr} = \sigma_Y S. \tag{16}$$

Reinforcement is not required if the peak elastic bending stress given by (12) does not exceed $\sigma_Y$.

*2.2. Case: Rectangular Slab Simply Supported at All Four Edges.* A rectangular slab simply supported at all four edges and uniformly loaded by blast pressure behaves as a two-way plate-like element. As in the one-way case, a small circular opening is assumed located within the slab where flexure predominates. The two-way rectangular slab and its deformed shape under blast loading are shown in Figures 9(a)–9(c).

Navier's method gives the exact solution for the deformed shape of a rectangular plate-like structure simply supported at all four edges and uniformly loaded by $q$; the solution is described by a rapidly converging double trigonometric series [39]. For simplicity, the first term in the series is employed to describe the deformed shape:

$$w(x, y) = \frac{16q \sin((\pi x)/\mathrm{b}) \sin((\pi \mathrm{y})/\mathrm{b})}{D\pi^6 ((1/\mathrm{b}^2) + (1/\mathrm{h}^2))^2}, \tag{17}$$

where $b$ is the slab width and $h$ is the slab length. The characteristic shape function is determined by multiplying (17) by its inverse whilst setting $x = b/2$ and $y = h/2$:

$$\varnothing(x, y) = \sin\left(\frac{\pi x}{b}\right) \sin\left(\frac{\pi y}{h}\right). \tag{18}$$

The bending stiffness corresponding to the out-of-plane displacement at the center of the slab is determined by substituting $q = 1$, $x = b/2$, and $y = h/2$ into the inverse of (17) and multiplying with the slab surface area:

$$K = \frac{D\pi^6 (b^2 + h^2)^2}{16 b^3 h^3}. \tag{19}$$

Finally, the mass and load transformation factors are determined by substituting (18) into the known formulas for transforming a multidegree system into an SDOF system [3]:

$$K_M = \frac{\int_0^h \int_0^b m\varnothing^2(x, y)\, dx\, dy}{mbh} = \frac{1}{4}, \tag{20a}$$

$$K_L = \frac{\int_0^h \int_0^b q\varnothing(x, y)\, dx\, dy}{qbh} = \frac{4}{\pi^2}, \tag{20b}$$

where $m$ is the mass density. In a manner similar to the one-way case, (19), (20a), and (20b) may be used to transform the load-structure system into an equivalent SDOF system and analyzed for a given blast loading scenario. The peak

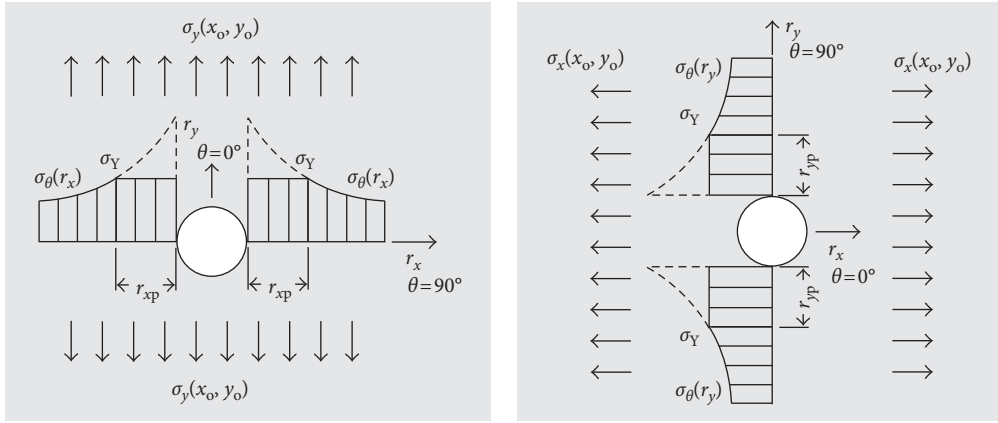


Figure 10: Far-field bending stress and resulting peak bending stress distribution along (a) $r_x$ and (b) $r_y$ directly adjacent to the circular opening.

displacement of the slab $\Delta_{peak}$ can be extracted for deformations remaining within the elastic strain range.

Substituting (18) into (8) and substituting the result into the Kirchhoff–Love plate differential equations given by (9a) and (9b) results in the bending stress field at the surface of the slab in tension:

$$\sigma_x(x_o, y_o) = \frac{6D\Delta_{peak}\pi^2 \sin((\pi x_o)/b)\sin((\pi y_o)/h)(b^2\mu + h^2)}{t^2b^2h^2}, \tag{21a}$$

$$\sigma_y(x_o, y_o) = \frac{6D\Delta_{peak}\pi^2 \sin((\pi x_o)/b)\sin((\pi y_o)/h)(b^2 + h^2\mu)}{t^2b^2h^2}, \tag{21b}$$

where $x_o$ is the location of the opening along the width of the slab and $y_o$ is its location along the length of the slab.

In the case of two-way flexure, the distribution of peak bending stress at the surface of the slab and directly adjacent to the opening is dependent upon the far-field bending stress in both the $x$-axis and $y$-axis directions, as shown in Figure 10 [38]. The peak elastic bending stress distribution, $\sigma_\theta(r_x)$, along the $r_x$ radial distance is principally induced by the far-field bending stress in the $y$-axis direction. Conversely, $\sigma_\theta(r_y)$ along the $r_y$ radial distance is principally induced by the far-field bending stress in the $x$-axis direction. The peak elastic bending stress distributions along $r_x$ and $r_y$ are obtained from (11) using the combinations of $\sigma_\infty$ and $\theta$ tabulated in Table 2.

Substituting the combinations of $\sigma_\infty$ and $\theta$ as tabulated in Table 2 into (11) results in the following equations:

$$\sigma_\theta(r_x) = -\frac{9D\pi^2\Delta_{peak}}{r_x^4t^2b^2h^2}\sin\left(\frac{\pi x_o}{b}\right)\sin\left(\frac{\pi y_o}{h}\right) \cdot \left(a^4 + \frac{a^2r_x^2}{3} + \frac{2r_x^4}{3}\right)\left(h^2\mu + b^2\right), \tag{22a}$$

$$\sigma_\theta(r_y) = \frac{9D\pi^2\Delta_{peak}}{r_y^4t^2b^2h^2}\sin\left(\frac{\pi x_o}{b}\right)\sin\left(\frac{\pi y_o}{h}\right) \cdot \left(a^4 + \frac{a^2r_y^2}{3} + \frac{2r_y^4}{3}\right)\left(h^2 + b^2\mu\right). \tag{22b}$$

The peak elastic bending stress distributions along $r_x$ and $r_y$ directly adjacent to the opening are depicted in Figure 10.

For the case of two-way flexure, reinforcement should be positioned on each side of the circular opening as required (Figure 11). Each region of reinforcement should be designed to transfer the concentrated peak bending moment, $M_{xp}$ or $M_{yp}$, on each side of the opening such that yielding does not occur at the wall surface. In accordance with the principle of conservation of mechanical energy given by (4), the concentrated peak bending moment producing a plastic hinge is derived by integrating the peak elastic bending stress distribution (assuming no yielding) over the radial distance over which yielding does occur and multiplying with the unit elastic section modulus:

$$M_{xp} = \frac{t^2}{6}\int_a^{r_{xp}+a}\sigma_\theta(r_x)\,dr_x, \tag{23a}$$

$$M_{yp} = \frac{t^2}{6}\int_a^{r_{yp}+a}\sigma_\theta(r_y)\,dr_y, \tag{23b}$$

where $r_{xp} + a$ and $r_{yp} + a$ are the radial distances at which $\sigma_\theta = \sigma_Y$. In summation form,

Table 2: Combinations of $\sigma_\infty$ and $\theta$ for use in (11) for obtaining the peak bending stress distributions along the $r_x$ and $r_y$ radial distances.

| Peak bending stress distribution | Plane stress distribution obtained from (11) | Uniaxial far-field tensile stress, $\sigma_\infty$, obtained from (21) | Angle, $\theta$, with respect to the axis of far-field stress |
|---|---|---|---|
| $\sigma_\theta(r_x)$ | $\sigma_\theta(r_x, \theta_y)$ | $\sigma_y$ | 90° |
| $\sigma_\theta(r_y)$ | $\sigma_\theta(r_y, \theta_x)$ | $\sigma_x$ | 90° |

$$M_{x\mathrm{p}} = \frac{t^2}{6} \sum_{i=a}^{r_{x\mathrm{p}}+a} \sigma_\theta(r_x)_i \Delta r_x, \tag{24a}$$

$$M_{y\mathrm{p}} = \frac{t^2}{6} \sum_{i=a}^{r_{y\mathrm{p}}+a} \sigma_\theta(r_y)_i \Delta r_y. \tag{24b}$$

The radial distances $r_{x\mathrm{p}}$ and $r_{y\mathrm{p}}$ over which yielding occurs can be solved for by substituting the known constants into (22a) and (22b), setting the results equal to $\sigma_\mathrm{Y}$, solving for $r_x$ and $r_y$, and subtracting $a$. Equations (22a) and (22b) may then be substituted into (24a) and (24b) to obtain the concentrated peak bending moments. The summation terms in (24a) and (24b) may be readily solved in spreadsheet form by summing the values of $\sigma_\theta$ at each incremental length $\Delta r_x$ or $\Delta r_y$ along the radial distance $r_{x\mathrm{p}}$ or $r_{y\mathrm{p}}$, respectively.

As in the one-way case, the nominal elastic bending limit $M_{\mathrm{nr}}$ of each reinforced region directly adjacent to the opening should be equal to or greater than the corresponding concentrated peak bending moment demand, $M_{x\mathrm{p}}$ or $M_{y\mathrm{p}}$, as expressed by the fundamental design requirement given by (15). The widths of the reinforced regions resisting $M_{x\mathrm{p}}$ and $M_{y\mathrm{p}}$ should nominally be equal to $r_{x\mathrm{p}}$ and $r_{y\mathrm{p}}$, respectively, and extend longitudinally to at least beyond the extents of the opening, as shown in Figure 11. Reinforcement is not required if the peak elastic bending stress given by (22a) and (22b) does not exceed $\sigma_\mathrm{Y}$.

The derived formulas (12), (14), (22a), (22b), (24a), and (24b) employ several assumptions for the purpose of functionality. The formulas assume isotropic homogeneous, linear elastic-perfectly plastic material properties and neglect the elastoplastic transition phase through the plate-like structure thickness. The former assumption is accurate for most metallic structural materials such as alloy steel but less applicable for anisotropic nonhomogeneous materials such as reinforced concrete [38]. The latter assumption is sufficient for relatively thin plate-like structures having a thickness-to-length ratio ranging between 0.1 and 0.01 [41]. Additionally, the approach of using the plane stress obtained from the Kirchhoff–Love plate equations for loading a circular opening in an infinite plane neglects the influence of nearby edge supports. However, this is compensated in that reinforcement around openings near edge supports should be designed primarily for shear rather than flexure; openings in regions where flexure predominates are more accommodating to the assumption of an infinite plane. Finally, the formulas apply only for blast load global responses remaining primarily within the elastic strain range. Consequently, the method is inherently elemental; however, the method is acquiescent to further analytical or empirical refinement.

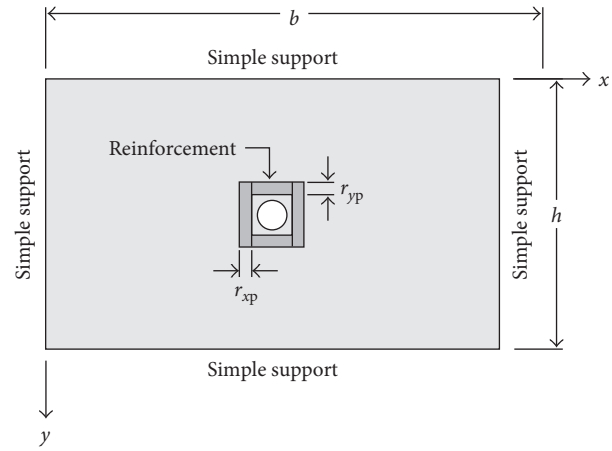


Figure 11: Reinforcement arrangement around a circular opening in the two-way rectangular slab.

*2.3. FEA Verification of Analytical Solution.* Abaqus was used to perform numerical verification of the peak elastic bending stress distribution formulas given by (12), (22a), and (22b). A series of plate-like structures each containing a small circular opening were modeled using general purpose S4R shell elements to verify the formulas. The global mesh size was set to 10 cm, with a much finer mesh size of 0.20 cm defined in the immediate region around the circular opening. The typical test model configuration is shown Figure 12. Eight test groups each containing three test models were analyzed considering various design parameters including blast loading conditions, model dimensions, material properties, positions of opening, and support conditions. The design parameters are summarized in Tables 3 and 4. Idealized isotropic homogeneous, linear elastic material properties were assigned to the shell sections as outlined in Table 5.

The blast effects software ConWep was used to calculate the peak reflected pressure and impulse upon each model considering various explosive charge weights and range to the target surface as listed in Table 6. The reflecting surface was set equal to the target surface to account for clearing effects [42]. Triangular blast pressure-time histories were developed based on the calculated pressure and impulse and used as a basis for determining the design parameters. The design parameters were optimized such that the blast load response remained within the elastic strain range. The typical blast loading scenarios are depicted in Figure 13.

The primary objective of the test groups was to demonstrate a correlation between the derived peak elastic bending stress distribution formulas and the FEA results. This is also indirect verification of the concentrated peak bending moments given by (14), (24a), and (24b), and the

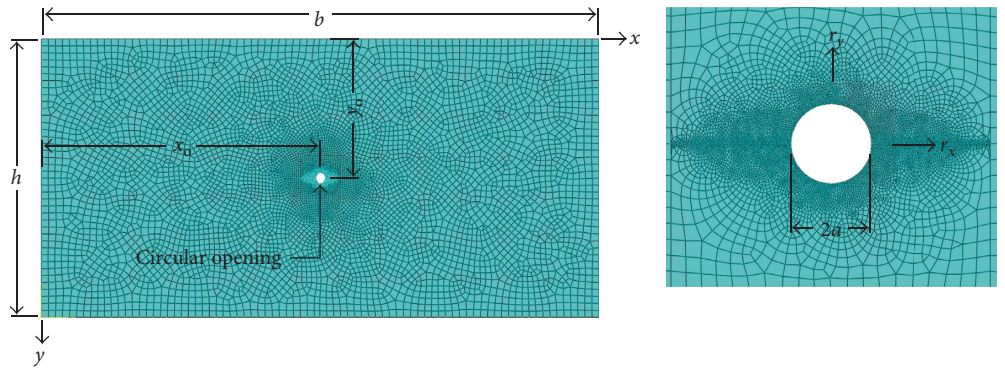


(a) (b)

Figure 12: Typical test model configuration: (a) test model mesh; (b) fine mesh around opening.

Table 3: Test group properties.

| Test group | Support conditions | Material[1] | Width, $b$ (m) | Height, $h$ (m) | Circular hole diameter, $2a$ (cm) | Circular hole location, $x_o$ (m) | Circular hole location, $y_o$ (m) |
|---|---|---|---|---|---|---|---|
| TM-1 | One-way | Carbon steel | 8 | 4 | 15 | 4 | 2 |
| TM-2 | One-way | Carbon steel | 8 | 4 | 15 | 4 | 1 |
| TM-3 | One-way | Titanium | 8 | 4 | 25 | 4 | 2 |
| TM-4 | One-way | Titanium | 8 | 4 | 25 | 4 | 1 |
| TM-5 | Two-way | Carbon steel | 8 | 4 | 15 | 4 | 2 |
| TM-6 | Two-way | Carbon steel | 8 | 4 | 15 | 6 | 1 |
| TM-7 | Two-way | Titanium | 10 | 8 | 30 | 5 | 4 |
| TM-8 | Two-way | Titanium | 10 | 8 | 30 | 8 | 2 |

[1]Refer to Table 5 for material properties.

Table 4: Test model thicknesses.

| Test model | Thickness, $t$ (cm) |
|---|---|
| TM-1a | 4 |
| TM-1b | 6 |
| TM-1c | 8 |
| TM-2a | 4 |
| TM-2b | 6 |
| TM-2c | 8 |
| TM-3a | 2 |
| TM-3b | 3 |
| TM-3c | 4 |
| TM-4a | 2 |
| TM-4b | 3 |
| TM-4c | 4 |
| TM-5a | 4 |
| TM-5b | 6 |
| TM-5c | 8 |
| TM-6a | 4 |
| TM-6b | 6 |
| TM-6c | 8 |
| TM-7a | 3 |
| TM-7b | 4 |
| TM-7c | 5 |
| TM-8a | 3 |
| TM-8b | 4 |
| TM-8c | 5 |

corresponding peak elastic strain energy developed around the circular opening. Test groups TM-1 through TM-4 investigated the stress concentrations around the circular opening under one-way flexural behavior and were intended to simulate an idealized one-way hardened blast wall. Test groups TM-5 through TM-8 investigated the stress concentrations under two-way flexural behavior and were intended to simulate an idealized two-way strengthened slab. The peak elastic bending stress distribution formulas specifically assume isotropic homogeneous, linear elastic material properties, and consequently, the test groups were modeled with such material properties for the purpose of impartial comparison with the formulas. The intention was therefore not to scrupulously simulate the real-life behavior of the considered test models but rather to investigate the correlation of the derived formulas with FEA whilst considering the aforementioned design parameters.

Three steps were defined in Abaqus for the analysis of each test model. In the first step, the support conditions were defined. In the second step, a dynamic implicit step was created with a duration equal to the blast load duration. The appropriate triangular pressure-time history was built into the load definition and uniformly applied to the model surface representing the target area. History output requests for the out-of-plane displacement and stress field around the

Table 5: Test model shell element material properties [40, 43].

| Material | Yield strength, $\sigma_Y$ (MPa) | Young's modulus, $E$ (GPa) | Poisson's ratio, $\nu$ | Density, $\rho$ (kg/m$^3$) |
|---|---|---|---|---|
| Carbon steel | 345 | 200 | 0.30 | 7860 |
| Titanium | 880 | 114 | 0.34 | 4430 |

Table 6: Blast pressure and impulse imposed upon test groups.

| Test group | Equivalent TNT charge mass (kg) | Range to target (m) | Uniform peak pressure[1] (kPa) | Uniform impulse[1] (kPa·msec) |
|---|---|---|---|---|
| TM-1 | 500 | 50 | 63.61 | 592.54 |
| TM-2 | 500 | 50 | 63.61 | 592.54 |
| TM-3 | 350 | 40 | 76.19 | 614.05 |
| TM-4 | 350 | 40 | 76.19 | 614.05 |
| TM-5 | 450 | 65 | 39.59 | 409.96 |
| TM-6 | 450 | 65 | 39.59 | 409.96 |
| TM-7 | 275 | 60 | 34.82 | 382.45 |
| TM-8 | 275 | 60 | 34.82 | 382.45 |

[1]Reflecting surface set equal to the target surface to account for clearing effects.

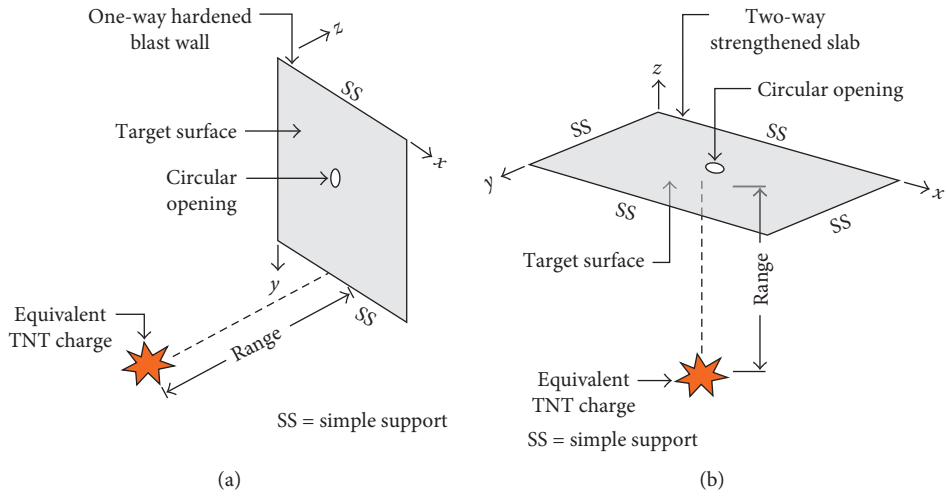


Figure 13: Typical blast loading scenarios: (a) test groups TM-1 through TM-4; (b) test groups TM-5 through TM-8.

opening were defined. In the final step, a second dynamic implicit step was created with a duration of 0.50 seconds and with a time step of 0.001 seconds to simulate the free vibration phase. The blast load was set to inactive, and the history output requests for the displacement and stress field around the opening were propagated from the second step. For each analysis, the history output requests for the displacement were used to determine the time step at which the peak displacement occurred. The peak unidirectional bending stress distribution at the tension surface and along $r_x$ or $r_y$ at that specific time step was then extracted from the analysis.

Concurrently, a series of dynamic SDOF blast analyses were performed on the test groups to replicate the analysis procedure that would be followed in the proposed method. For each test model, an SDOF analysis was conducted in order to obtain the peak out-of-plane displacement. The peak displacement was then substituted into (12), (22a), or (22b) and the resulting peak bending stress distribution along $r_x$ or $r_y$ was compared to the FEA results. Finally, the concentrated peak bending moments were calculated using (14), (24a), or (24b) for use in designing any required reinforcement around the circular openings. The overall numerical verification procedure is outlined in Figure 14.

## 3. Results and Discussion

The peak out-of-plane displacements from the equivalent undamped SDOF analyses and FEA are summarized in Table 7. The displacements were obtained at the center of each test model at $x = b/2$ and $y = h/2$. The typical displacement-time history is characterized by undamped periodic motion in the $z$-axis direction, as exemplified in Figure 15(a) for the test model TM-1c. The peak displacement is achieved at the first peak during the free vibration phase. For the one-way test models, the SDOF analyses slightly underestimate the peak displacements compared to FEA. The percentage difference between SDOF and FEA tends to reduce as the thickness of the plate-like structure increases. Conversely, the SDOF analyses overestimate the

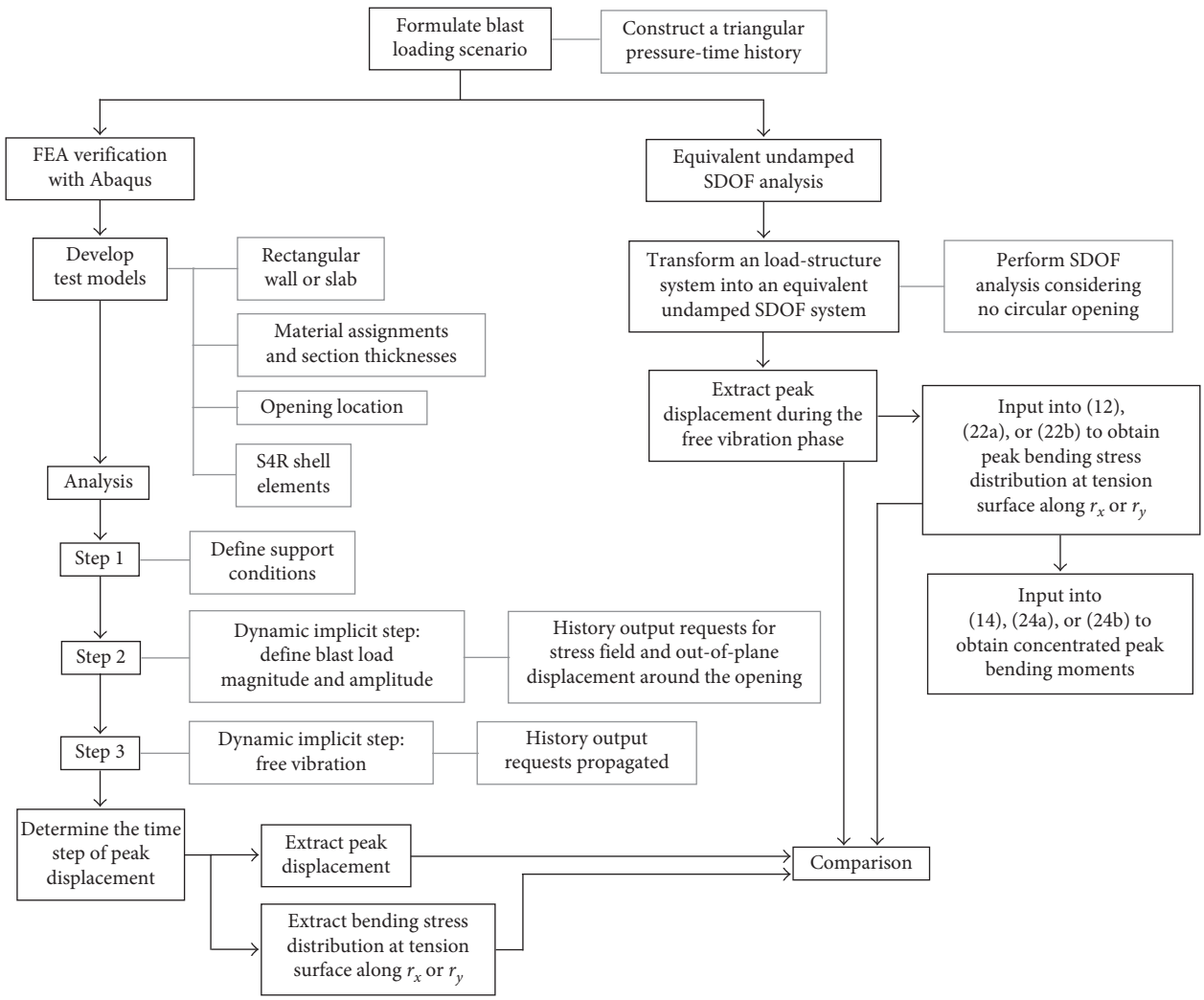


Figure 14: Numerical verification procedure.

peak displacements for the two-way test models compared to FEA, and the percentage difference tends to increase as the thickness increases. These minor differences may be derived from the slight differences in global stiffness between the SDOF models and the FEA models. The stiffness in the FEA models is in part dependent upon the fineness of mesh and accounts for the presence of the circular opening. On the contrary, the stiffness in the SDOF models is in part dependent upon the assumed deformed shape and neglects the presence of the opening. It is noted that, as per the proposed analysis method and verification procedure, both the SDOF and FEA models were analyzed without considering reinforcement in order to predict the unaltered (i.e., unreinforced) performance of the plate-like structures.

Equations (12), (22a), and (22b) predicting the peak bending stress distributions around the opening are directly dependent upon the peak out-of-plane displacement. In this way, these formulas can be directly coupled to the peak displacement response of a preceding dynamic SDOF blast analysis to readily design any required reinforcement around a circular opening. Typical bending stress contours are shown in Figures 15(b) and 15(c) for the test model TM-1c. The peak bending stress distributions along $r_x$ as obtained from (12) and FEA are shown in Figure 16 for the one-way test groups TM-1 through TM-4. The stress distributions along $r_x$ and $r_y$ as obtained from (22a) and (22b), respectively, and FEA are shown in Figures 17 and 18 for the two-way test groups TM-5 through TM-8. Equation (12) demonstrates a good correlation with the FEA results. Equations (22a) and (22b) tend to slightly overestimate the stress concentrations compared to FEA. The correlation is strongest when the opening is located in regions where flexural stress predominates (Figures 6 and 9). As may be expected, the correlation decreases as the opening approaches any edge supports by virtue of the supports having an increasing influence upon the far-field bending stress. In all cases, the derived formulas predict slightly greater stress concentrations directly adjacent to the opening perimeter compared to FEA. Overall, the formulas exhibit closer correlation to the FEA results for the one-way test models than for the two-way models. There is no apparent correlation between the test model thickness and the correlation of stress concentrations.

Table 7: Peak displacement from SDOF and FEA.

| Test model | SDOF $\Delta_{peak}$ (cm) | FEA $\Delta_{peak}$ (cm) | % difference |
|---|---|---|---|
| *One-way test models* | | | |
| TM-1a | 10.3 | 12.3 | 17.7 |
| TM-1b | 4.51 | 5.36 | 17.2 |
| TM-1c | 2.48 | 2.89 | 15.3 |
| TM-2a | 10.3 | 12.3 | 17.7 |
| TM-2b | 4.51 | 5.33 | 16.7 |
| TM-2c | 2.48 | 2.87 | 14.6 |
| TM-3a | 76.2 | 92.8 | 19.6 |
| TM-3b | 33.8 | 40.2 | 17.3 |
| TM-3c | 18.9 | 22.5 | 17.4 |
| TM-4a | 76.2 | 90.9 | 17.6 |
| TM-4b | 33.8 | 39.7 | 16.1 |
| TM-4c | 18.9 | 22.2 | 16.1 |
| *Two-way test models* | | | |
| TM-5a | 10.8 | 9.34 | 14.5 |
| TM-5b | 4.64 | 3.89 | 17.6 |
| TM-5c | 2.54 | 1.96 | 25.8 |
| TM-6a | 10.8 | 9.35 | 14.4 |
| TM-6b | 4.64 | 3.89 | 17.6 |
| TM-6c | 2.49 | 1.96 | 23.8 |
| TM-7a | 97.3 | 78.1 | 21.9 |
| TM-7b | 54.6 | 44.1 | 21.3 |
| TM-7c | 34.9 | 28.1 | 21.6 |
| TM-8a | 97.3 | 76.8 | 23.5 |
| TM-8b | 54.6 | 43.1 | 23.5 |
| TM-8c | 34.9 | 27.6 | 23.4 |

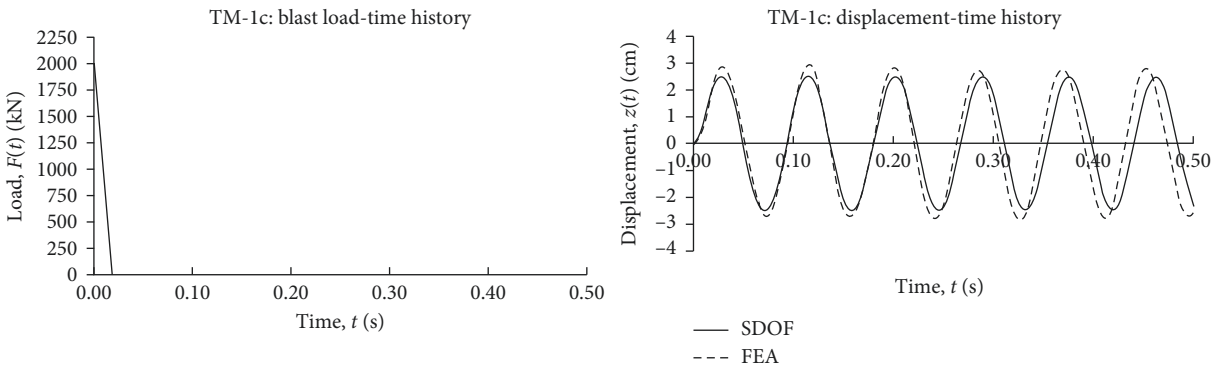


(a)

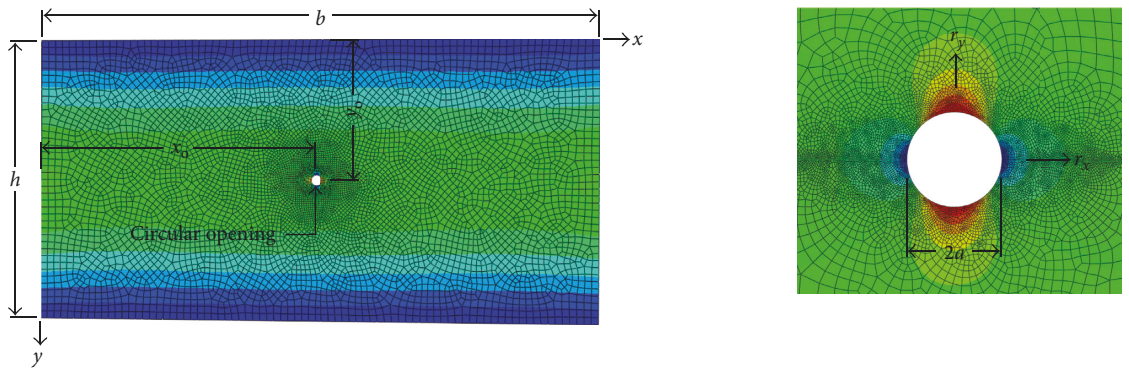


(b) (c)

Figure 15: Test model TM-1c SDOF and FEA analysis results: (a) blast load time history and corresponding displacement-time history from SDOF and FEA; (b) bending stress contours in the $y$-axis direction on the tension surface of TM-1c; (c) stress contours around the opening.

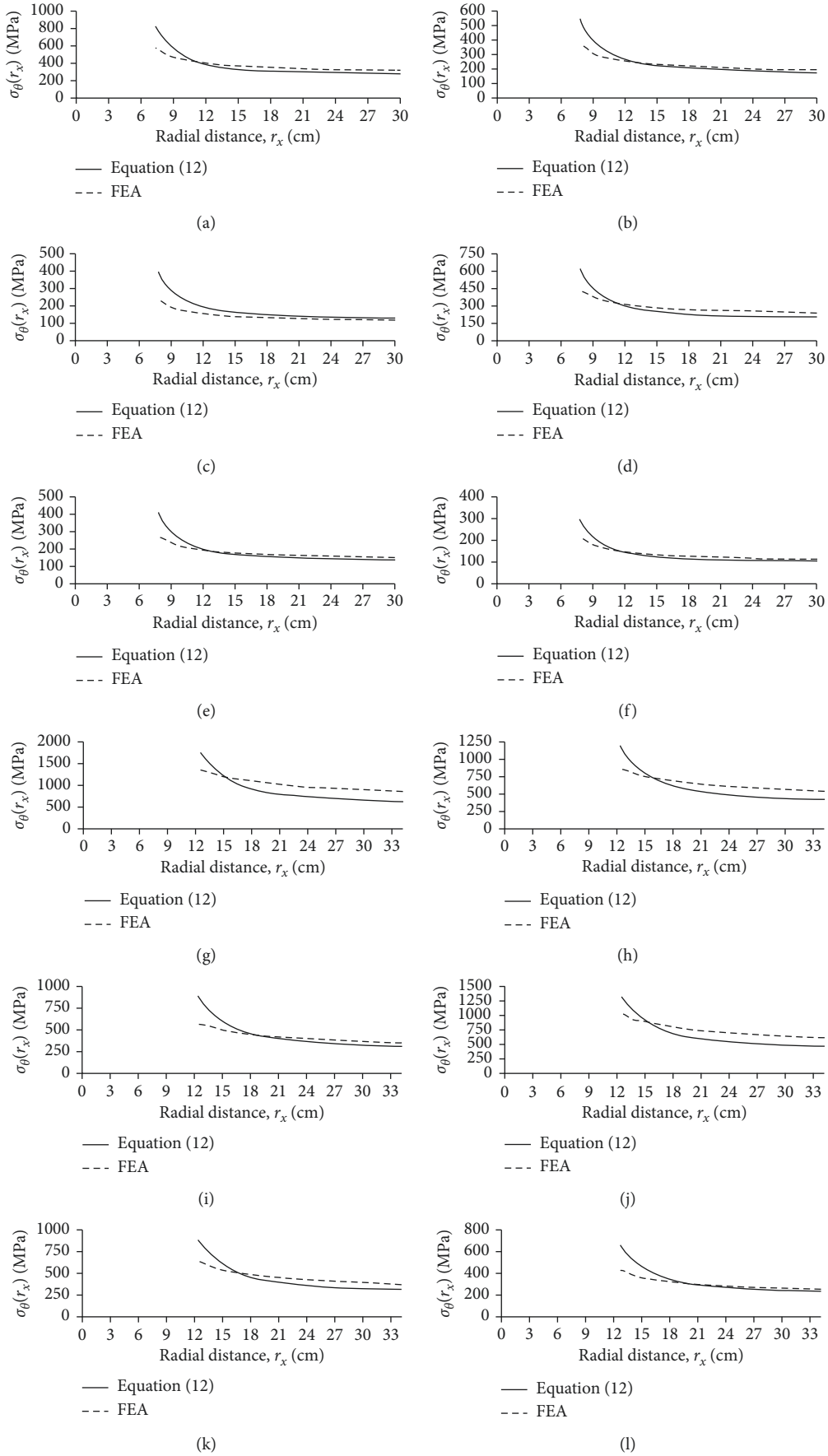


Figure 16: Comparison of (12) and FEA derived peak bending stress distributions along $r_x$ for the test groups TM-1 through TM-4 (one-way test models): (a) TM-1a; (b) TM-1b; (c) TM-1c; (d) TM-2a; (e) TM-2b; (f) TM-2c; (g) TM-3a; (h) TM-3b; (i) TM-3c; (j) TM-4a; (k) TM-4b; (l) TM-4c.

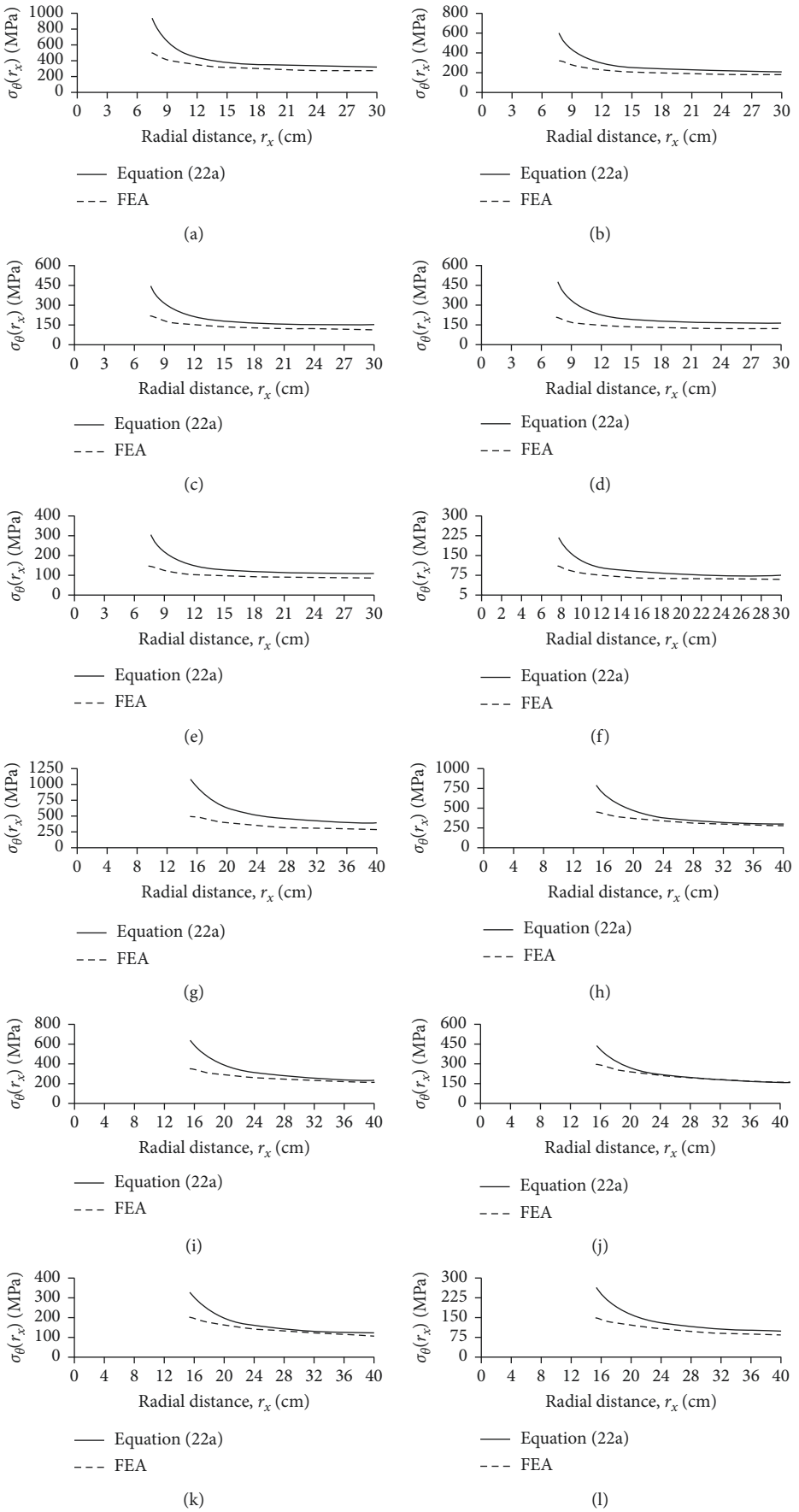


Figure 17: Comparison of (22a) and FEA derived peak bending stress distributions along $r_x$ for the test groups TM-5 through TM-8 (two-way test models): (a) TM-5a; (b) TM-5b; (c) TM-5c; (d) TM-6a; (e) TM-6b; (f) TM-6c; (g) TM-7a; (h) TM-7b; (i) TM-7c; (j) TM-8a; (k) TM-8b; (l) TM-8c.

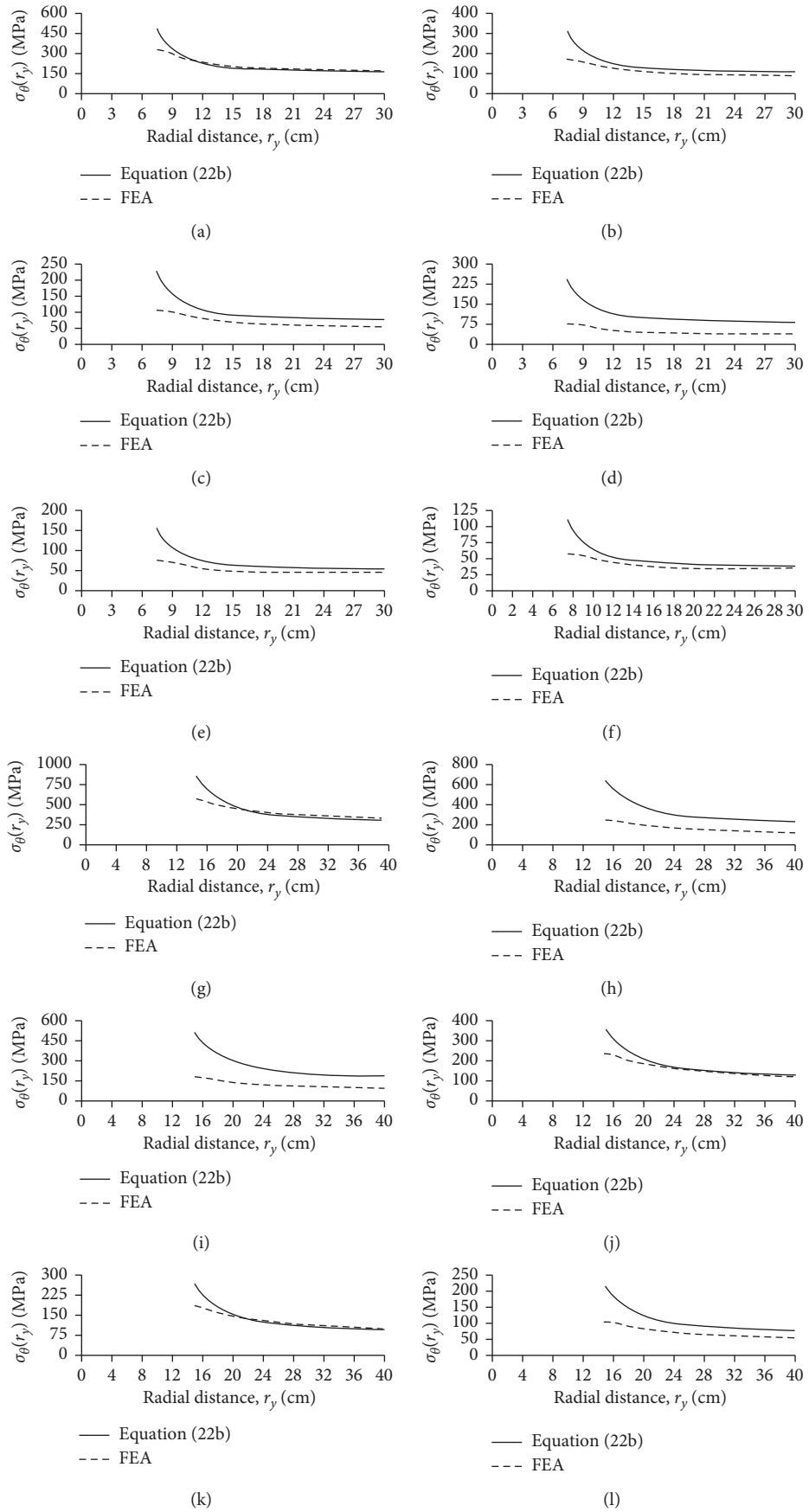


Figure 18: Comparison of (22b) and FEA derived peak bending stress distributions along $r_y$ for the test groups TM-5 through TM-8 (two-way test models): (a) TM-5a; (b) TM-5b; (c) TM-5c; (d) TM-6a; (e) TM-6b; (f) TM-6c; (g) TM-7a; (h) TM-7b; (i) TM-7c; (j) TM-8a; (k) TM-8b; (l) TM-8c.

Table 8: Concentrated peak bending moments for the one-way test models.

| Test model | $M_{xp}$ per (14) (kN·m) |
|---|---|
| TM-1a | 8.34 |
| TM-1b | 4.88 |
| TM-1c | 1.97 |
| TM-2a | 3.37 |
| TM-2b | 1.34 |
| TM-2c | NR |
| TM-3a | 5.24 |
| TM-3b | 2.89 |
| TM-3c | NR |
| TM-4a | 2.07 |
| TM-4b | 0.13 |
| TM-4c | NR |

NR = no reinforcement required.

Table 9: Concentrated peak bending moments for the two-way test models.

| Test model | $M_{xp}$ per (24a) (kN·m) | $M_{yp}$ per (24b) (kN·m) |
|---|---|---|
| TM-5a | 15.8 | 5.70 |
| TM-5b | 7.53 | NR |
| TM-5c | 4.19 | NR |
| TM-6a | 1.39 | NR |
| TM-6b | NR | NR |
| TM-6c | NR | NR |
| TM-7a | 2.03 | NR |
| TM-7b | NR | NR |
| TM-7c | NR | NR |
| TM-8a | NR | NR |
| TM-8b | NR | NR |
| TM-8c | NR | NR |

NR = no reinforcement required.

The concentrated peak bending moments given by (14), (24a), and (24b) for the one-way and two-way test groups are listed in Tables 8 and 9, respectively. These formulas are directly dependent upon (12), (22a), and (22b). As per the principle of conservation of mechanical energy given by (4), if the peak elastic bending stress concentrations in the local domain around a circular opening are accurate, then the concentrated peak bending moments derived from the distributions can allow for the design of reinforcement to absorb the peak strain energy $\Delta U_{\text{peak}}$ around the opening in a purely elastic form. The summation term in the formulas was readily solved in spreadsheet form by summing the stress magnitude at each incremental length $\Delta r$ along the radial distance $r_{xp}$ or $r_{yp}$. Considering that the elastoplastic transition range through the plate-like structure thickness is neglected in the derivation of (14), (24a), and (24b), the formulas may slightly overestimate the values of $M_{xp}$ and $M_{yp}$. In accordance with the design requirement expressed by (15), this may result in a conservative design of the reinforcement.

An inclination towards conservatism in design is generally favorable, especially with respect to blast design since the nominal, unreduced capacities are used [1]. Nonetheless, the results show that many of the test models do not require reinforcement by virtue of the peak bending stress concentrations not exceeding the material yield strength. The concentrated bending moments tend to decrease when the opening is located in regions near edge supports where flexural stresses begin to decrease.

The design of steel reinforcement for the test model TM-2a is outlined as a typical example. For reinforced regions with rectangular cross sections and composed of isotropic homogeneous, linear elastic-perfectly plastic material, the elastic bending limit $M_{\text{nr}}$ is given as follows:

$$M_{\text{nr}} = \frac{\sigma_{\text{Y}} r_{\text{p}} d^2}{6}, \tag{25}$$

where $r_{\text{p}}$ is the width of the reinforced section equal to $r_{xp}$ or $r_{yp}$ and $d$ is the total thickness of the reinforced section. From Table 8, the magnitude of $M_{xp}$ for the test model TM-2a is 3.37 kN·m. Also, from Figure 16, the value of $r_{xp}$ is approximately 2.7 cm. As per the fundamental design requirement given by (15), the required thickness of the rectangular reinforced section can be readily determined by setting (25) equal to $M_{xp} = 3.37$ kN·m, substituting in the known material yield strength of $\sigma_{\text{Y}} = 345$ MPa, setting $r_{\text{p}} = 2.7$ cm, and solving for $d$. The required thickness of the reinforced section is solved to be $d = 4.7$ cm. By contrast, the nonreinforced thickness of the test model TM-2a is $t = 4$ cm. The final idealized reinforced sections on each side of the opening are depicted in Figure 19.

## 4. Conclusions

An analysis method is formulated for predicting the peak bending stress concentrations around a small circular opening in a plate-like structure subjected to uniform blast loading. The method is applicable to plate-like structures possessing isotropic homogeneous material properties and assumes a linear elastic-perfectly plastic response mode. Specifically, the method allows for the determination of concentrated peak bending moments adjacent to the opening for the design of reinforcement that can prevent the formation of localized plasticity. In terms of mechanical energy, the reinforced regions are designed to absorb the peak strain energy around the opening in a purely elastic form. This is under the supposition that the development of localized plasticity around the opening is the failure criterion. Specifically, the kinetic energy of the plate-like structure may progressively dissipate or build up as plastic strain energy around the opening, potentially resulting in large deformations, rupture, or dynamic fracture during the initial cycle or subsequent oscillations [34–36].

A set of elemental formulas is derived to achieve this objective, focusing upon rectangular one-way and two-way plate-like structures containing a single small circular opening located where flexure predominates. The formulas are those expressed by (12), (14), (22a), (22b), (24a), and (24b) and are directly dependent upon the predicted peak displacement response of a blast load-structure system. In conformance with the proposed method, the formulas are intended to be implemented in tandem with a dynamic SDOF analysis of the blast load-structure system.

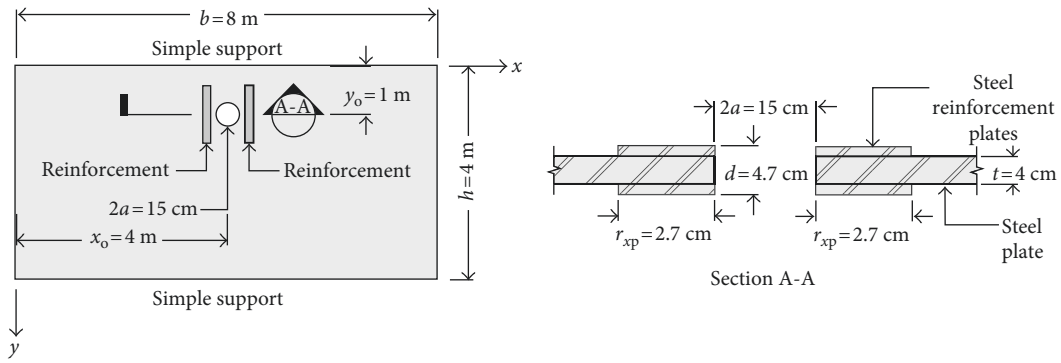


Figure 19: Idealized reinforced sections on each side of the opening for the test model TM-2a.

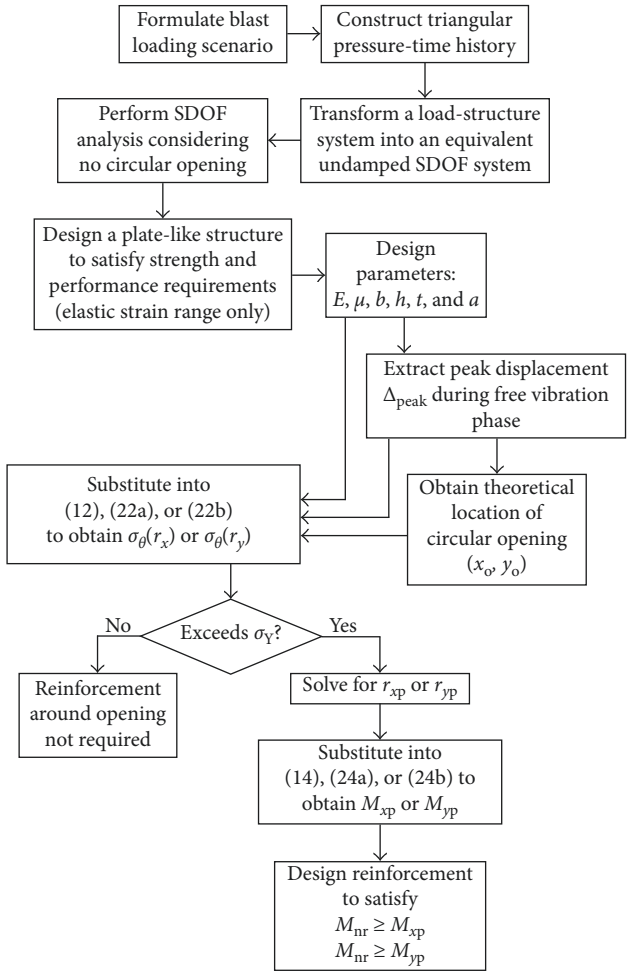


Figure 20: Proposed analysis and design method.

The deformed shape, characteristic shape function, stiffness, and transformation factors for a rectangular two-way flexural element are formulated. These same parameters are readily available in the literature for rectangular one-way flexural elements [3]. The proposed method is outlined in Figure 20 and can be readily incorporated into standard SDOF blast design spreadsheets.

Abaqus was employed to conduct FEA verification of the derived peak elastic bending stress distribution formulas. A total of 24 test models subdivided into eight test groups were investigated considering various design parameters. Overall, the formulas demonstrate a good correlation with FEA albeit with a conservative inclination; the formulas tend to slightly overestimate the stress concentrations directly adjacent to the opening perimeter compared to FEA. Additionally, the formulas neglect the elastoplastic transition phase through the plate-like structure thickness, which serves to add to the aforementioned conservatism. However, this conservatism is deemed favorable especially with regard to blast design.

The method is limited insomuch by the blast load-structure configuration that can be analyzed by way of an equivalent SDOF system. This is because the method is directly dependent upon the peak displacement response, deformed shape, characteristic shape function, and stiffness inherent to a dynamic SDOF analysis. The method is, however, acquiescent to further analytical or empirical refinement by future investigations or experiments to extend its applicability. Future studies could investigate the presence of multiple openings in a plate-like structure and openings with irregular shapes. The method could also be refined to accommodate plate-like structures composed of anisotropic nonhomogeneous materials.

The overall premise of the analysis method is to provide a more efficient and viable alternative than overgeneralized analytical methods or high fidelity FEA for analyzing and designing reinforcement around a circular penetration located in a plate-like structure subjected to uniform blast loading. The proposed method is applicable for many typical conditions that may be encountered during design. With further modifications, the method has the potential to be applicable for an even wider range of structural configurations, with the remaining atypical conditions reserved for analysis by FEA.

## Data Availability

The data used to support the findings of this study are available from the corresponding author upon request.

## Conflicts of Interest

The authors declare that there are no conflicts of interest regarding the publication of this paper.

## References


[1] ASCE 59-11, *Blast Protection of Buildings*, American Society of Civil Engineers, Reston, VA, USA, 2011.

[2] N. M. Newmark, "An engineering approach to blast resistant design," *Transactions of the American Society of Civil Engineers*, vol. 121, pp. 45–64, 1956.

[3] J. M. Biggs, *Introduction to Structural Dynamics*, McGraw-Hill, New York, NY, USA, 1964.

[4] C. Mayrhofer, "Reinforced masonry walls under blast loading," *International Journal of Mechanical Sciences*, vol. 44, no. 6, pp. 1067–1080, 2002.

[5] M. Poulin, C. Viau, D. N. Lacroix, and G. Doudak, "Experimental and analytical investigation of cross-laminated timber panels subjected to out-of-plane blast loads," *Journal of Structural Engineering*, vol. 144, no. 2, article 04017197, 2018.

[6] Y. E. Ibrahim, M. A. Ismail, and M. Nabil, "Response of reinforced concrete frame structures under blast loading," *Procedia Engineering*, vol. 171, pp. 890–898, 2017.

[7] M. Larcher, M. Arrigoni, C. Bedon et al., "Design of blast-loaded glazing windows and facades: a review of essential requirements towards standardization," *Advances in Civil Engineering*, vol. 2016, Article ID 2604232, 14 pages, 2016.

[8] X. Zhang and C. Bedon, "Vulnerability and protection of glass windows and facades under blast: experiments, methods and current trends," *International Journal of Structural Glass and Advanced Materials Research*, vol. 1, no. 2, pp. 10–23, 2017.

[9] A. Kadid, "Stiffened plates subjected to uniform blast loading," *Journal of Civil Engineering and Management*, vol. 14, no. 3, pp. 155–161, 2008.

[10] A. Vatani Oskouei and F. Kiakojouri, "Steel plates subjected to uniform blast loading," *Applied Mechanics and Materials*, vol. 108, pp. 35–40, 2012.

[11] D. Ambrosini and A. Jacinto, "Numerical-experimental study of steel plates subjected to blast loading," *WIT Transactions on Engineering Sciences*, vol. 49, pp. 49–62, 2005.

[12] H. R. Tavakoli and F. Kiakojouri, "Numerical dynamic analysis of stiffened plates under blast loading," *Latin American Journal of Solids and Structures*, vol. 11, no. 2, pp. 185–199, 2014.

[13] J. Y. Park, E. Jo, M. S. Kim, S. J. Lee, and Y. H. Lee, "Dynamic behavior of a steel plate subjected to blast loading," *Transactions of the Canadian Society for Mechanical Engineering*, vol. 40, no. 4, pp. 575–583, 2016.

[14] K. Cichocki and U. Perego, "Rectangular plates subjected to blast loading: the comparison between experimental results, numerical analysis and simplified analytical approach," *Le Journal de Physique IV*, vol. 7, pp. C3-761–C3-766, 1997.

[15] L. A. Loucaa and Y. G. Pana, "Response of stiffened and unstiffened plates subjected to blast loading," *Engineering Structures*, vol. 20, no. 12, pp. 1079–1086, 1998.

[16] M. D. Goel, V. A. Matsagar, and A. K. Gupta, "Dynamic response of stiffened plates under air blast," *International Journal of Protective Structures*, vol. 2, no. 1, pp. 139–155, 2011.

[17] A. C. Jacinto, R. D. Ambrosini, and R. F. Danesi, "Dynamic response of plates subjected to blast loading," *Structures and Buildings*, vol. 152, no. 3, pp. 269–276, 2002.

[18] S. E. Rigby, A. Tyas, and T. Bennett, "Elastic-plastic response of plates subjected to cleared blast loads," *International Journal of Impact Engineering*, vol. 66, pp. 37–47, 2014.

[19] UFC (United Facilities Criteria) 3-340-02, *Structures to Resist the Effects of Accidental Explosions*, U.S. Army Corp of Engineers, Naval Facilities Engineering Command, Air Force Civil Engineer Support Agency, Panama City, FL, USA, 2008.

[20] E. G. Kirsch, "Die theorie der elastizität und die bedürfnisse der festigkeitslehre," *Zeitschrift des Vereines deutscher Ingenieure*, vol. 42, pp. 797–807, 1898.

[21] A. G. Griffith, "The phenomena of rupture and flow in solids," *Philosophical Transactions of the Royal Society A: Mathematical, Physical and Engineering Sciences*, vol. 221, pp. 163–198, 1921.

[22] H. M. Westergaard, "Bearing pressures and cracks," *Journal of Applied Mechanics*, vol. 6, pp. A49–A53, 1939.

[23] G. Irwin, "Analysis of stresses and strains near the end of a crack traversing a plate," *Journal of Applied Mechanics*, vol. 24, pp. 361–364, 1957.

[24] L. Toubal, M. Karama, and B. Lorrain, "Stress concentration in a circular hole in composite plate," *Composite Structures*, vol. 68, no. 1, pp. 31–36, 2005.

[25] M. Batista, "On the stress concentration around a hole in an infinite plate subject to a uniform load at infinity," *International Journal of Mechanical Sciences*, vol. 53, no. 4, pp. 254–261, 2011.

[26] M. Jafari and E. Ardalani, "Stress concentration in finite metallic plates with regular holes," *International Journal of Mechanical Sciences*, vol. 106, pp. 220–230, 2016.

[27] N. Momcilovic, M. Motok, and T. Maneski, "Stress concentration on the contour of a plate opening: analytical, numerical and experimental approach," *Journal of Theoretical and Applied Mechanics*, vol. 51, no. 4, pp. 1003–1012, 2013.

[28] P. E. Erickson and W. F. Riley, "Minimizing stress concentrations around circular holes in uniaxially loaded plates," *Experimental Mechanics*, vol. 18, no. 3, pp. 97–100, 1978.

[29] S. Ghuku and K. Saha, "An experimental study on stress concentration around a hole under combined bending and stretching stress field," *Procedia Technology*, vol. 23, pp. 20–27, 2016.

[30] S. M. Ibrahim and H. McCallion, "Elastic stress concentration factors in finite plates under tensile loads," *The Journal of Strain Analysis for Engineering Design*, vol. 1, no. 4, pp. 306–312, 1966.

[31] C. J. Brown, A. L. Yattram, and M. Burnett, "Stability of plates with rectangular holes," *Journal of Structural Engineering*, vol. 113, no. 5, pp. 1111–1116, 1987.

[32] E. Maiorana, C. Pellegrino, and C. Modena, "Elastic stability of plates with circular and rectangular holes subjected to axial compression and bending moment," *Thin-Walled Structures*, vol. 47, no. 3, pp. 241–255, 2009.

[33] M. A. Komur and M. Sonmez, "Elastic buckling behavior of rectangular plates with holes subjected to partial edge loading," *Journal of Constructional Steel Research*, vol. 112, pp. 54–60, 2015.

[34] H. Yang, S. K. Sinha, Y. Feng, D. B. McCallen, and B. Jeremic, "Energy dissipation analysis of elastic-plastic materials," *Computer Methods in Applied Mechanics and Engineering*, vol. 331, pp. 309–326, 2018.

[35] N. Aravas, K. S. Kim, and F. A. Leckie, "On the calculations of the stored energy of cold work," *Journal of Engineering Materials and Technology*, vol. 112, pp. 465–470, 1990.

[36] A. Shukla, *Practical Fracture Mechanics in Design*, Marcel Dekker, New York, NY, USA, 2nd edition, 2005.

[37] R. R. Craig Jr. and A. J. Kurdila, *Fundamentals of Structural Dynamics*, John Wiley & Sons, Hoboken, NJ, USA, 2006.

[38] M. H. Sadd, *Elasticity: Theory, Applications, and Numerics*, Academic Press, Burlington, MA, USA, 2nd edition, 2009.

[39] S. Timoshenko and S. Woinowsky-Krieger, *Theory of Plates and Shells*, McGraw-Hill, New York, NY, USA, 2nd edition, 1987.

[40] F. P. Beer, E. R. Johnston Jr., and J. T. DeWolf, *Mechanics of Materials*, McGraw-Hill, New York, NY, USA, 4th edition, 2006.
[41] E. Ventsel and T. Krauthammer, *Thin Plates and Shells: Theory, Analysis, and Applications*, Marcel Dekker, New York, NY, USA, 2001.
[42] A. Tyas, J. A. Warren, T. Bennett, and S. D. Fay, "Prediction of clearing effects in far-field blast loading of finite targets," *Shock Waves*, vol. 21, no. 2, pp. 111–119, 2011.
[43] R. Boyer, G. Welsch, and E. W. Collings, *Material Properties Handbook: Titanium Alloys*, ASM International, Materials Park, OH, USA, 1994.